BIBECHANA
Vol. 23, No. 2, April 2026, 93-99

ISSN 2091-0762 (Print), 2382-5340 (Online)
Journal homepage: http://nepjol.info/index.php/BIBECHANA
Publisher:Dept. of Phys., Mahendra Morang A. M. Campus (Tribhuvan University)Biratnagar

Spatial orientation of angular momentum vectors: a comparative study of i–band spirals in SDSS Redshift slices 0.13-0.14 and 0.14-0.15

Obihang Kandangwa, Prem Bahadur Karki, Janak Ratna Malla*

Department of Physics, Amrit Science Campus, Tribhuvan University, Nepal.

*Corresponding authors: Email: janak.malla@ac.tu.edu.np

Abstract

This paper presents comparative studied of the spatial orientation of angular momentum alignment of 20,000 spiral galaxies selected from the SDSS DR16 i–band photometry. The sample is divided into two intermediate redshift ranges: $0.13-0.14$ *and* $0.14-0.15$*. The 2D parameters were converted into 3D spin orientations using Godlowskian transformation, where the azimuthal angle is derived from the tangential formula. A "Virtual Control" simulation of* 10^7 *random galaxies was developed in the model of the survey to predict the expected distribution. Statistical analyses were performed to evaluate the randomness of the distributions. The statistical results show that while localized anisotropies exist in specific slices, the overall orientation of spin vectors is consistent with isotropy. The Fourier coefficients for both samples fall within the Hierarchy model of galaxy formation.*

Keywords
Orientation, angular momentum vector, SDSS, Godlowskian transformation, Hierarchy model.

Article information
Manuscript received: January 29, 2026; Revised: March 10, 2026; Accepted: April 26, 2026
DOI https://doi.org/10.3126/bibechana.v23i2.90213

1 Introduction

According to the cosmological principle, the universe is homogeneous and isotropic on a sufficiently large scale [1]. However, on smaller scales this uniformity breaks down, and we observe a complex 'Cosmic Web' composed of galaxy clusters, superclusters, filaments, and vast voids [2, 3]. One important way to investigate galaxy formation is to study the standard model of cosmic structure formation. Galaxies acquire spins during their early protogalactic stage through gravitational torques exerted by surrounding matter. This is known as Tidal Torque Theory (TTT). The theory predicts that a galaxy's spin direction is not arbitrary but depends on the tidal forces of the immediate large-scale structure [4]. Therefore, spiral galaxy orientations serve as a kind of fossil record reflecting the dynamical state of the universe shortly before galaxies fully formed [5]. Different galaxy orientation scenarios predict different galaxies formation theories. The Hierarchy model having randomized orientations predicts bottom–up formation [4]. The Pancake Model having parallel spin to the plane of structure predicts top–down formation [6]. And the Primordial Turbulence Model, having perpen-

dicular spin to the plane of the structure, predicts turbulent formation [7].

Despite many years of observation, results on galaxy alignments often remain contradictory. Methodologically, the field was standardized by Hawley and Peebles [8], who introduced the statistical tests used to assess isotropy. While studies of the Local Supercluster reported significant alignments with the plane of the local Supercluster [9], some research suggests that environmental factors play a decisive role [10, 11]. Aryal et al. [12, 13] and Malla et al. [14, 15] have investigated galaxy orientations across various sky regions and redshift depths. Their work reveals that while localized alignments can be found within specific filaments or clusters, the broader population generally supports the Hierarchy model [2, 3]. The deeper fields are often less certain. A significant advancement in this field is the introduction of virtual control samples. Focusing on narrow redshift intervals is vital in understanding if these alignments evolve over cosmic history or remain static.

This research uses data from the 16th data release of the Sloan Digital Sky Survey (SDSS DR16) [16], focusing on i-band data. Our sample consists of galaxies in the intermediate redshift range 0.13<z<0.15, which allows us to select clean slices of the cosmic web. We then search for alignment using the statistical methods standardized by Hawley and Peebles [7, 17].

2 Data and Method

2.1 Data

In this study, we extracted necessary data of the spiral galaxies from the 16th data release of the Sloan Digital Sky Survey (SDSS DR16) [16], which can be accessed through https://www.sdss.org/dr16//. We selected 10,000 of the brightest galaxies in two distinct redshift slices, 0.13-0.14 and 0.14-0.15. To ensure the robust comparison of the spiral galaxies only in both slices, we modified the SQL where class= 'GALAXY',fracDeV<0.7 to select spirals and early spiral galaxies, expAB>0.2 to ensure the axial ratio is greater than the intrinsic flatness, and petroR90>1.5" to resolve the galaxies radially. The SQL used to extract our data from SDSS and a subset of large data is shown in appendix A and B section, respectively.

2.2 Methods

2.2.1 Inclination angle

We used the standard formula for the oblate spheroids proposed by Holmberg to calculate the inclination angle (i) [18]. For q=b/a (axial ratio) and q*= 0.2 (intrinsic flatness) for oblate spirals, we have:

$$\cos^2 i = \frac{q^2 - q^{*2}}{1 - q^{*2}} \tag{1}$$

2.2.2 Godlowskian transformation

The raw SDSS coordinates right ascension (α), declination (δ) and the position angles (p) are in the equatorial frame. These were converted into Super Galactic (SG) coordinates right ascension (L), declination (B) and position angle (P). For 3D orientation of the galaxy spin vectors, we calculated the polar angle (θ) and the azimuthal angle(ϕ). The polar angle (θ) represents the inclination of the galaxy spin vector with respect to the SG plane, ranging from 0° to 90°. The azimuthal angle(ϕ) represents the projection of the spin vector onto the SG plane, varying between -90° to 90°. We used the Flin and Godłowski method (hereafter the F&G method) to calculate the angular spin vector (θ, ϕ) [9].

$$\sin\theta = -\cos i \sin B \pm \sin i \sin P \cos B \tag{2}$$

$$N_x = -\cos i \cos B \cos L + \sin i \begin{pmatrix} \mp \sin P \sin B \cos L \\ \pm \cos P \sin L \end{pmatrix} \tag{3}$$

$$N_y = -\cos i \cos B \sin L + \sin i \begin{pmatrix} \mp \sin P \sin B \sin L \\ \mp \cos P \cos L \end{pmatrix} \tag{4}$$

From Equations (3) and (4), we obtain:

$$\tan\phi = \frac{N_y}{N_x} \tag{5}$$

We specifically used the tangent formula to ensure all angles in all quadrants are preserved.

2.3 Statistical testing

According to cosmological principle, the universe is homogeneous and isotropic on a sufficiently large scale. So, in our case, when we create 107 virtual galaxy to satisfy cosmology principle in excel file. So, we generated 107 virtual galaxies to estimate the expected distribution within 18 bins for directional ambiguity. We compute the observed counts in each of the18 bins of 5° step size for and 10° step size for. Comparison and various statistical testing of the observed data are done against the virtual expected model to assess the randomness of the distribution. Galaxy clusters do not show an obvious alignment when looking at pictures, so we used statistical analysis to check preferred alignments. Let Nk be the number of observed galaxies in the k-th bin and N0k be the expected number of galaxies in the same k-th bin. In this work, we used:

2.3.1 Chi-square test (χ^2)

It measures the deviation of the observed distribution from the expected random distribution. It is calculated as:

$$\chi^2 = \sum_{k=1}^{n} \frac{(N_k - N_{0k})^2}{N_{0k}} \quad (6)$$

We reject isotropy for P (>) < 0.05.

2.3.2 Auto-correlation (C)

It quantifies the correlation between counts of galaxies in adjacent bins.

$$C = \sum_{k=1}^{n} \frac{(N_k - N_{0k})(N_{k+1} - N_{0\,k+1})}{\sqrt{N_{0k} N_{0\,k+1}}} \quad (7)$$

The distribution is anisotropic for $\frac{C}{\sqrt{n}} > 1$.

2.3.3 First-order Fourier test

It determines the direction of the preferred alignment [19].

$$\Delta_{11} = \frac{\sum_{k=1}^{n} (N_k - N_{0k}) \cos(2\theta_k)}{\sum_{k=1}^{n} N_{0k} \cos^2(2\theta_k)} \quad (8)$$

For $\frac{\Delta_{11}}{\sigma(\Delta_{11})}$ between −1.5 and 1.5, it supports the Hierarchy model; > 1.5 supports the Parallel Pancake model, and < −1.5 supports the Perpendicular Turbulence model [19].

2.4 Data calculations and plotting

All the calculations and virtual simulations are done with the help of MATLAB7.0.1. The statistical analysis is performed with EXCEL2019, and the plotting and graphs are made from ORIGIN5.0 and ORIGIN8.0.

3 Results and discussion

Both the slices are named correspondingly: Sample i34 for 0.13 < z < 0.14 and Sample i45 for 0.14 < z <0.15.

3.1 Observable parameters

Prior to the 3D spin vector, the 2D parameters should be considered between both slices., and p are successfully transformed into L, B, and P, as seen in Figure 1. The similarity of the observed coordinates in both slices is the survey masks of the SDSS. The PAs are expected to be uniform in all the frames.

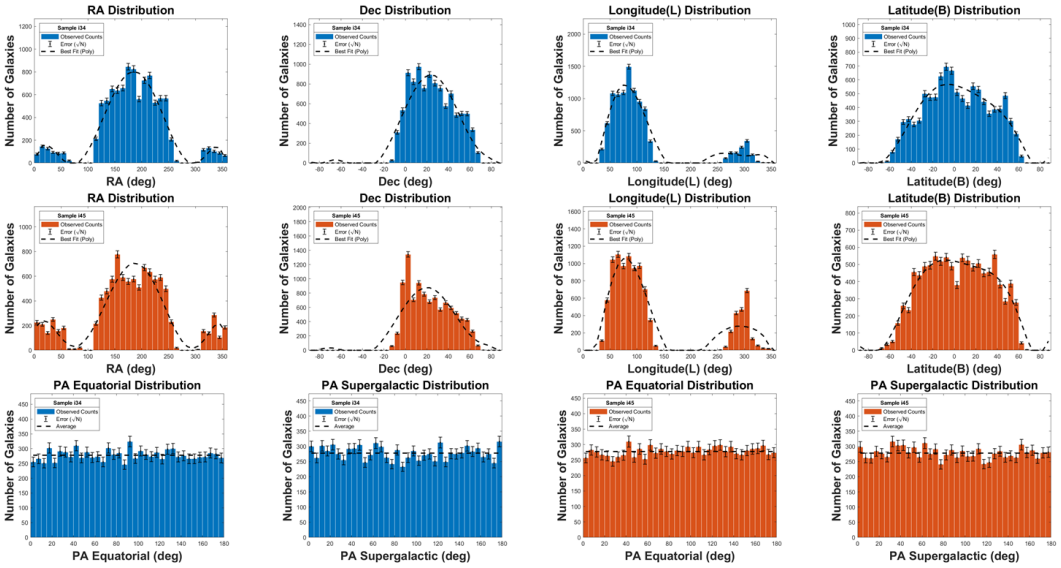

Figure 1: Observable parameters in Sample i34 (blue colour) and Sample i45 (red colour) in both the equatorial and SG coordinate systems.

3.2 Sample properties

It is essential to confirm whether variation in alignment signals is not due to sample selection effects. Physical properties of our sample galaxies must be ascertained before further calculation.The axial ratio distribution (1st column) shows a cutoff below 0.2, which verifies our SQL criteria (Figure 2). Inclination angle (2nd column) follows the expected Gaussian-like distribution for both samples. The i-magnitude distribution (3rd column) has higher counts of fainter galaxies and is well within the limitation of the SDSS telescope. The redshift distributions (4th column) confirm that all galaxies lie well within our sample boundaries.

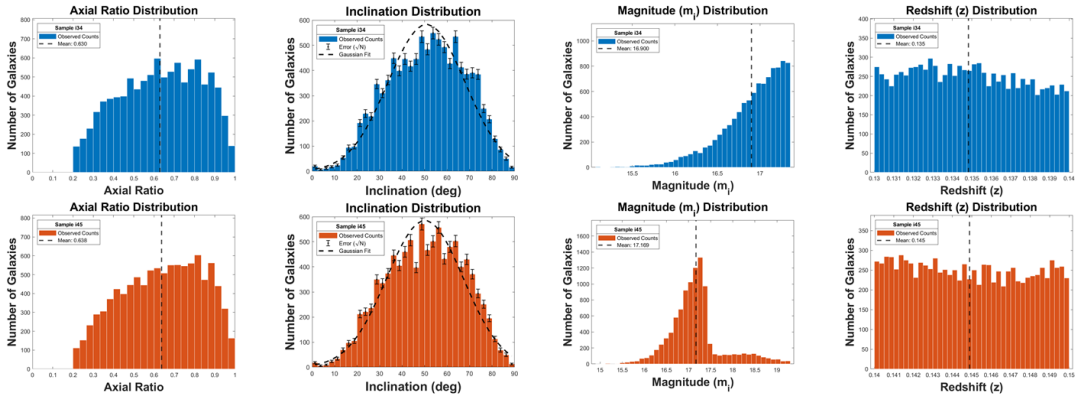

Figure 2: Physical Properties in Sample i34 (blue colour) and Sample i45 (red colour).

3.3 Geometric distribution

The conversion of the equatorial coordinate system to the SG coordinate system can be analyzed as a sky map distribution. Figure 3 compares the distribution of galaxies for Sample i34 in both coordinate systems. In the equatorial frame the galaxies are concentrated at the North Galactic Cap, seen as a large continuous patch around =180°. This is a typical observation pattern of the SDSS telescope. While in the SG frame, this patch is rotated and shifted toward L=0°. The color scale represents the redshift (z), illustrating the depth of the survey.Sample i45 (not shown) exhibits a nearly identical geometric distribution.

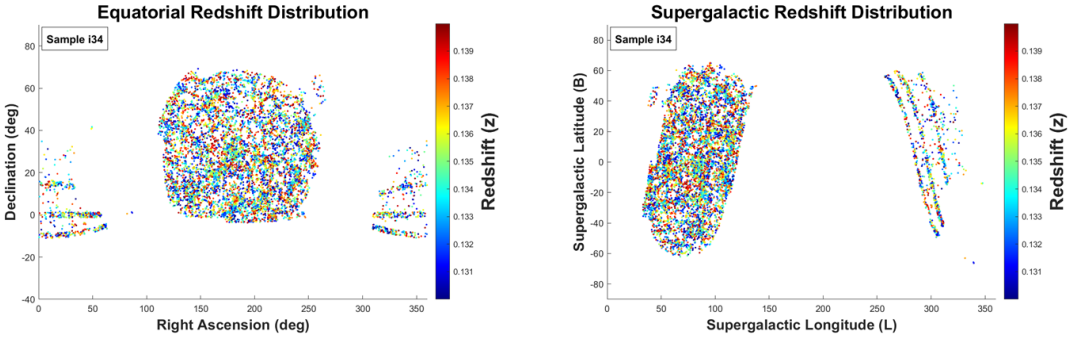

Figure 3: Redshift Sky map of Sample i34 on both equatorial (left) and SG (right) frames.

3.4 Galaxy's spin vectors: Polar angle (θ) and azimuthal angle (ϕ)

illustrates the polar angle distribution (1st column) and azimuthal angle distribution (2nd column) of observed (red dots with error bars), control expectation (black line), and theoretical isotropic distributions (dotted blue line) graphically, Figure 4. For polar angle, the expected curve for both samples follows theoretical cosine-like distributions. The observed counts closely follow the expected curve in both samples with minor dips (52.5°, 62.5°) in Sample i34 and humps (12.5°) and dips (2.5°, 27.5°) in Sample i45.

For azimuthal angle, the expected curve has a non-uniform u-shape with minima centered near =0°. Despite the non-uniformity, the data fluctuates around the average line, which may be caused by the limitation of the survey. The observed data closely mirror the expected non-uniformity with minor local humps and dips in both samples. The overall trend may seem consistent with the geometric expectation with few deviations, but the contribution of the humps and dips needs to be verified through statistical tests to assess randomness.

3.5 Statistical Analysis

Table 1 summarizes the statistical results for both the samples. For Sample i34, Chi-Square probability (0.06 for θ and 0.77 for ϕ) indicates that the observed distributions do not significantly deviate from the isotropic expectation at the 5% level. In Sample i45, the azimuthal distribution remains consistent with isotropy (0.20), whereas the polar distribution shows a statistically significant deviation (0.01). Autocorrelation results suggest local-

ized anisotropies between adjacent bins in the polar angle of Sample i34 (-1.71) and azimuthal angles of Sample i45 (-1.65). Despite minor localized fluctuations and anisotropies, the first-order Fourier coefficients for all cases fall within the -1.5 to 1.5 range. This indicates there is no dominance of large-scale preferred alignment pointing toward the Hierarchy model of the galaxy orientations.

Table 1: Statistical results for both samples

Parameter	Sample i34		Sample i45	
	θ	ϕ	θ	ϕ
$P(>\chi^2)$	0.06	0.77	0.01	0.20
$C/\sigma(C)$	-1.71	-0.12	0.19	-1.65
$\Delta_{11}/\sigma(\Delta_{11})$	0.31	-0.89	-0.35	-0.98

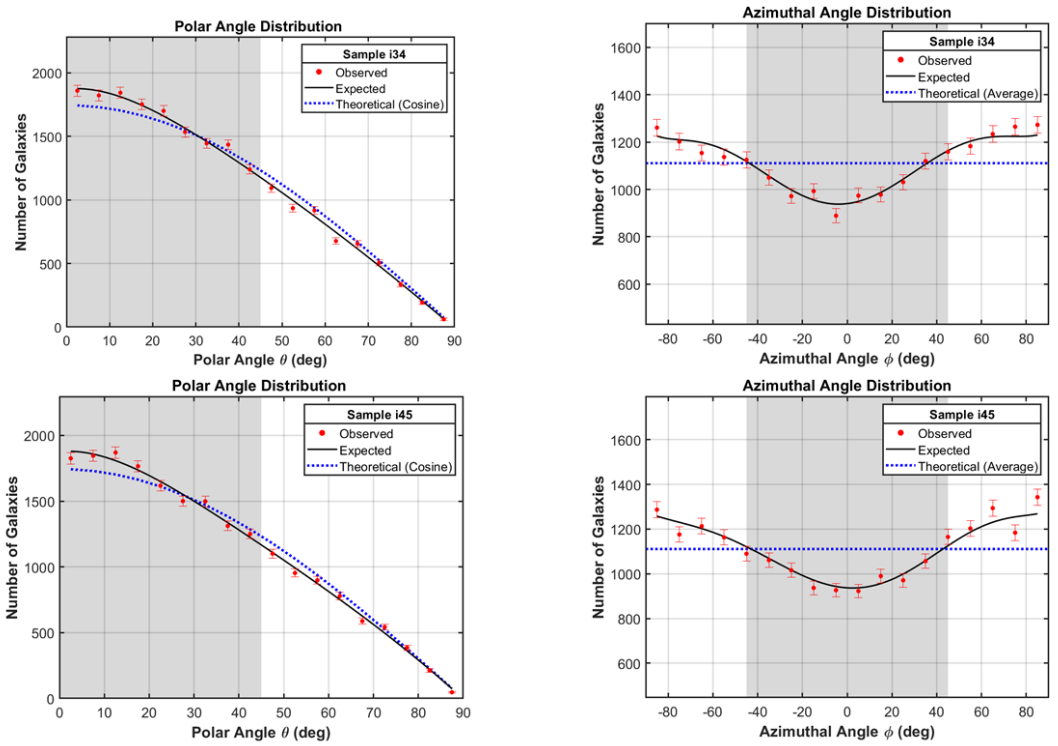

Figure 4: Comparative plot between observed, expected, and theoretical curves for polar angles (1st column) and azimuthal angles (2nd column) in Sample i34 (1st row) and Sample i45 (2nd row).

4 Conclusion

We have presented a comparative analysis of the angular momentum orientation of spiral galaxies within two adjacent redshift slices ($0.13 < z < 0.15$). We verified the selection criteria of the spiral galaxies through plotting. By utilizing a virtual control simulation, we demonstrated the expected survey mask of the azimuthal distribution. The statistical evaluation of the spin vectors revealed a statistically significant deviation from the isotropy only in the polar distribution for Sample i45, while Sample i34 remained consistent with a random distribution. Additionally, autocorrelation tests detected localized anisotropies (bin-specific fluctuation) in the polar angles of Sample i34 and azimuthal angles of Sample i45. However, the first-order Fourier analysis suggested the Hierarchy Model. We conclude that the spin vectors of spiral galaxies in these redshift slices are generally randomized. They favor a "bottom-up" scenario of structure formation where galaxies acquire angular momentum through tidal torque during the protogalactic stage.

5 Acknowledgement

The authors would like to acknowledge the Sloan Digital Sky Survey (SDSS) for making the DR16 dataset publicly available. These data were fundamental to this research.

References

[1] Gonçalves RS, et al. Cosmic homogeneity: a spectroscopic and model-independent measurement. Monthly Notices of the Royal Astronomical Society Letters. 2018;475:L20-4.

[2] Aluri PK, et al. Is the observable Universe con-

sistent with the cosmological principle? Classical and Quantum Gravity. 2022;39:204001.

[3] Cautun M, et al. Evolution of the cosmic web. Monthly Notices of the Royal Astronomical Society. 2014;441:2923-73.

[4] Peebles PJE. Origin of the Angular Momentum of Galaxies. Astrophysical Journal. 1969;155:393.

[5] Doroshkevich AG. Spatial structure of perturbations and origin of galactic rotation in fluctuation theory. Astrophysics. 1970;6:320-30.

[6] Zel'dovich YB. Gravitational instability: An approximate theory for large density perturbations. Astronomy and Astrophysics. 1970;5:84-9.

[7] Ozernoy LM. The whirl theory of the origin of structure in the universe. In: The Large Scale Structure of the Universe: Symposium No. 79; 1978. p. 427-38.

[8] Hawley DL, Peebles PJE. Distribution of observed orientations of galaxies. Astronomical Journal. 1975;80:477-91.

[9] Flin P, Godłowski W. The orientation of galaxies in the Local Supercluster. Monthly Notices of the Royal Astronomical Society. 1986;222:525-41.

[10] Jones BJT, et al. Fossil evidence for spin alignment of Sloan Digital Sky Survey galaxies in filaments. Monthly Notices of the Royal Astronomical Society. 2010;408:897-918.

[11] Zhang B, et al. Alignments between Galaxies and the Cosmic Web at z 1–2 in the IllustrisTNG Simulations. Astrophysical Journal. 2023;954:49.

[12] Aryal B, Saurer W. Spin vector orientations of galaxies in eight Abell clusters of BM type I. Astronomy and Astrophysics. 2004;425:871-9.

[13] Aryal B, et al. Spatial orientation of angular momentum vector of galaxies in three merging binary clusters. Astrophysics and Space Science. 2012;337:313-9.

[14] Malla JR, et al. Spatial orientation of galaxies in supercluster S [227+006+0078]. BIBECHANA. 2020;17:117-22.

[15] Malla JR, et al. Spatial orientations of angular momentum vectors of galaxies in Supercluster S [173+014+0082]. BIBECHANA. 2021;18:26-32.

[16] Ahumada R, et al. The 16th Data Release of the Sloan Digital Sky Surveys. Astrophysical Journal Supplement Series. 2020;249:3.

[17] Godłowski W, et al. The Orientation of Galaxies in Galaxy Clusters. Astrophysical Journal. 2010;723:985-95.

[18] Holmberg E. On the apparent diameters and the orientation in space of extragalactic nebulae. Meddelanden från Lunds Astronomiska Observatorium. 1946;117:3-82.

[19] Godłowski W. Remarks on the Methods of Investigations of Alignment of Galaxies. Astrophysical Journal. 2012;747:7.

Appendix A

```
SELECT TOP 10000
    p.objID, s.class, p.ra, p.dec,
    s.z AS redshift,
    p.modelMag_i - p.extinction_i AS mag_i,
    p.expAB_i, p.expPhi_i, p.petroR90_i
FROM Galaxy p
JOIN SpecObj s ON p.objID = s.bestObjID
WHERE
    p.clean = 1
    AND s.class = 'GALAXY'
    AND s.zWarning = 0
    AND s.z BETWEEN 0.13 AND 0.14   -- SLICE A
    -- AND s.z BETWEEN 0.14 AND 0.15 -- uncomment for slice B
    AND p.fracDeV_i < 0.7           -- Spirals
    AND p.expAB_i > 0.2             -- not too flat/edge-on
    AND p.petroR90_i > 1.5          -- size resolved
ORDER BY (p.modelMag_i - p.extinction_i) ASC;  -- Ascending
```

Appendix B

Table 2: Subset of data for Sample i34

objID	class	ra	dec	redshift	mag_i	expAB_i	expPhi_i	petroR90_i
1.23767E+18	GALAXY	173.273	59.33716	0.132829	15.06777	0.622743	59.31197	13.67271
1.23766E+18	GALAXY	168.2425	57.96138	0.133765	15.09248	0.900689	-10.5606	9.885622
1.23766E+18	GALAXY	147.16	36.91719	0.13171	15.11501	0.938881	12.38832	12.88211
1.23767E+18	GALAXY	242.1895	16.96563	0.131845	15.12244	0.765744	33.86491	10.71299
1.23765E+18	GALAXY	182.7202	6.179027	0.138473	15.15124	0.764291	122.2212	11.90519
1.23767E+18	GALAXY	242.0318	19.16828	0.136728	15.20445	0.714157	159.2799	13.30396
1.23766E+18	GALAXY	49.94954	-0.22114	0.131681	15.2505	0.544108	164.3009	10.74961
1.23766E+18	GALAXY	124.6669	55.43801	0.134395	15.25979	0.59004	-10.6996	10.18
1.23766E+18	GALAXY	177.9909	46.04229	0.135021	15.26865	0.678666	135.4263	9.422857
1.23766E+18	GALAXY	144.941	8.751082	0.136742	15.30111	0.632111	119.2126	10.28879
1.23767E+18	GALAXY	128.3047	17.26899	0.134425	15.30459	0.579177	58.43733	10.45172
1.23766E+18	GALAXY	224.0077	33.04136	0.133084	15.31924	0.261504	111.8874	9.896046
1.23766E+18	GALAXY	187.2132	3.869291	0.133996	15.34085	0.649857	35.86219	9.701068
1.23765E+18	GALAXY	220.4613	1.264357	0.137415	15.35263	0.55612	39.32001	13.05964
1.23767E+18	GALAXY	173.6113	21.32496	0.13007	15.35501	0.917179	99.81097	10.27117
1.23766E+18	GALAXY	181.401	37.84985	0.135944	15.37194	0.862301	172.7811	12.31709
1.23767E+18	GALAXY	179.6075	26.49804	0.138136	15.38068	0.722782	77.18114	13.95849
1.23766E+18	GALAXY	157.0383	39.23212	0.130316	15.4044	0.706774	7.828463	11.44869
1.23767E+18	GALAXY	173.273	59.33716	0.132829	15.06777	0.622743	59.31197	13.67271

Table 3: Subset of data for Sample i45

objID	class	ra	dec	redshift	mag_i	expAB_i	expPhi_i	petroR90_i
1.24E+18	GALAXY	228.9421	2.599061	0.140613	14.89763	0.272607	151.3855	16.66874
1.24E+18	GALAXY	244.6042	9.179067	0.147769	15.01623	0.585474	159.2865	15.51897
1.24E+18	GALAXY	132.5226	12.77424	0.149175	15.09384	0.583459	28.91385	11.02272
1.24E+18	GALAXY	205.3154	12.22621	0.143173	15.12632	0.574082	4.339816	8.551695
1.24E+18	GALAXY	223.5877	8.210157	0.142545	15.14576	0.77124	18.6972	11.50131
1.24E+18	GALAXY	177.1681	65.21392	0.145147	15.15066	0.820498	147.6272	10.62186
1.24E+18	GALAXY	155.9163	49.144	0.142156	15.17795	0.737536	81.40202	20.51719
1.24E+18	GALAXY	234.7536	21.3456	0.143734	15.18826	0.585211	100.4315	14.03591
1.24E+18	GALAXY	141.2076	40.64768	0.142203	15.20777	0.705164	63.69151	13.23681
1.24E+18	GALAXY	218.7872	55.0855	0.140634	15.29708	0.641053	146.3839	7.759304
1.24E+18	GALAXY	178.6032	24.08038	0.142476	15.37548	0.758181	125.2246	10.7549
1.24E+18	GALAXY	203.7532	58.71902	0.149202	15.39001	0.616218	184.5592	12.07451
1.24E+18	GALAXY	180.6157	33.30441	0.146938	15.42656	0.681708	3.91735	14.05373
1.24E+18	GALAXY	208.5253	17.83516	0.142602	15.44195	0.819606	89.39347	9.287654
1.24E+18	GALAXY	174.9735	34.11559	0.145551	15.4559	0.865466	128.3871	7.901419
1.24E+18	GALAXY	146.1846	38.78956	0.145889	15.46276	0.511972	89.99197	13.28347
1.24E+18	GALAXY	246.8164	7.901089	0.142991	15.46695	0.775725	16.10328	9.537233
1.24E+18	GALAXY	68.64373	25.282	0.144507	15.47322	0.564978	72.57062	5.430873
1.24E+18	GALAXY	19.39736	25.04116	0.143417	15.47468	0.618367	97.18291	19.51732